AIChE

Effect of Gas Evolution on Mixing and Conversion in a Flow-Through Electrochemical Reactor

Matthew A. Petersen and Kenneth F. Reardon
Dept. of Chemical and Biological Engineering, Colorado State University, Fort Collins, CO 80523

DOI 10.1002/aic.11827
Published online July 13, 2009 in Wiley InterScience (www.interscience.wiley.com).

Flow-through electrolytic reactors (FTER) emplaced below the subsurface may be used to control the migration of groundwater contamination away from source zones. During prior studies with FTERs, water electrolysis and associated gas generation have occurred concurrently with contaminant degradation. Gas evolution-induced mixing within the electrode assembly has the potential to impact system performance. A mathematical model of the system was developed to capture the impact of mixing on transport processes in the system. Corresponding transient and steady-state tracer experiments using ferricyanide as a model contaminant were conducted to quantify mixing-dependent parameters and verify modeling results. Over a range of relevant groundwater flowrates, Peclet numbers were between 0.1 and 10, indicating that mixing was a important process under low-flow conditions. Comparison of experiments and model calculations demonstrated that incorporating gas evolution into the model was necessary for accurate performance prediction. © 2009 American Institute of Chemical Engineers *AIChE J,* 55: 2468–2476, 2009
Keywords: electrochemical reactor, gas-evolving electrode, mixing, remediation, current efficiency

Introduction

Permeable reactive barriers (PRBs) have become a popular technology for controlling the migration of groundwater contamination away from source zones. Traditionally, PRBs have been constructed with a granular reactive medium (e.g., zero-valent iron[1,2]) placed in a trench to intercept a plume of groundwater contamination. The permeable medium allows the natural hydraulic gradient to transport contaminants through the system where they react to form environmentally benign compounds. Recently, we have focused on developing flow-through electrolytic reactors (FTER) as an option for in situ plume migration control.[3–5] Building on the conceptual design of a PRB, in an in situ FTER a set of closely spaced permeable mesh electrodes are substituted for the granular reactive medium. As groundwater passes through the electrodes the contaminants are degraded via oxidation and/or reduction reactions. FTERs offer some advantages over traditional PRBs, principally the ability to control surface reaction kinetics. The advantages of these systems make them compelling to explore further.

Process models that accurately predict how remediation systems behave as a function of operating conditions are important for both system design and analysis. Modeling PRBs constructed with granular media have traditionally used plug-flow[6,7] or numerical models[8,9] in conjunction with experimental observations[10–13] to analyze dispersion and non-uniform flow fields within the system. The large physical difference between FTERs and granular media-based PRBs requires a shift in the hydrodynamic and mass transport conceptual models of an in situ flow-through reactor.

For most of the conditions and contaminants we have evaluated, the reaction rates required to achieve significant removal of contaminants were attained at electrode potentials

Correspondence concerning this article should be addressed to K. F. Reardon at kenneth.reardon@colostate.edu

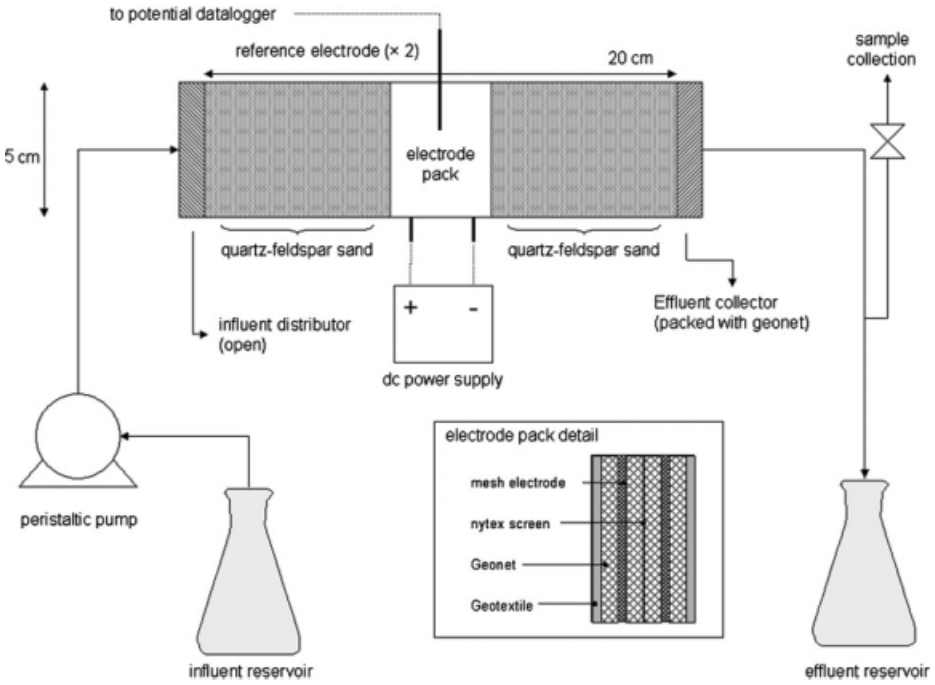

Figure 1. Schematic of the FTER experimental system.

sufficient for water electrolysis to occur. The central hypothesis of this research is that the effects of gas generation must be taken into account to correctly model FTER performance (i.e., contaminant conversion and selectivity) under relevant in situ operating conditions.

The objective of this research was to develop a macroscopic process model of an FTER. The effects of gas generation were incorporated into a one-dimensional reactor model. Model parameters for dispersion and reaction included the effects of gas generation. The one-electron reduction of ferricyanide ($Fe(CN)_6^{3-}$) to ferrocyanide ($Fe(CN)_6^{4-}$) was used as the model chemical system in a laboratory flow-through column reactor for parameter measurement and model verification in separate experiments.

Model Development

Basic reactor model

Key elements of an in situ FTER are presented in Figure 1. System components are discussed further in the experimental section of this article. The governing equation for a one-dimensional species balance around the electrode assembly for an arbitrary dilute reactant that undergoes the first-order unimolecular heterogeneous reaction is

$$\frac{dC_A}{dt} + u\frac{dC_A}{dx} = D\frac{d^2C_A}{dx^2} - kC_A \tag{1}$$

where t is time, u is the mass-average velocity in the x direction, C_A is the concentration of reactant A, x is the distance from the system inlet, D is the dispersion coefficient, and k is the reaction rate constant. The steady-state form of Eq. 1 was integrated over the system length (L) in the direction of flow using the closed-vessel (i.e., Danckwerts) boundary conditions, leading to the following expression for conversion

$$\chi_A = 1 - \frac{4a\exp\left(\frac{1}{2}Pe_m\right)}{(1+a)^2\exp\left(\frac{a}{2}Pe_m\right) - (1-a)^2\exp\left(-\frac{a}{2}Pe_m\right)} \qquad a = \sqrt{1 + 4k\tau(Pe_m)^{-1}} \tag{2}$$

where χ_A is the conversion of A, Pe_m ($= uL/D$) is a mixing Peclet number, and τ is the system residence time.[14] Building on these efforts, Eq. 2 was modified to address gas generation with our interest solely focused on the cathode chamber.

Model extension under gas evolution

The model parameters D and k in Eqs. 1 and 2 were modified to account for electrolytic gas generation. Gas generation and its effect on fluid mixing and mass transfer in electrochemical reactors has been examined under both static[15–18] and continuous flow processes.[19–23] Groundwater velocities are typically small and convection may play only a minor role in mass transport and the extent of mixing. Therefore, theoretical and empirical relationships developed for static systems were explored in addition to those reported for flow systems to modify model parameters.

The rate of gas generation was calculated assuming that only two reactions occurred at the cathode: the reduction of the reactant and the reduction of the solvent (water). The gas evolution rate may then be calculated as a function of current via Faraday's law.

$$Q_g = \frac{I}{A_E}(1 - \phi_A)\frac{RT}{n_S FP} \tag{3}$$

where Q_g is the surface area-normalized volumetric gas evolution rate, I is the current, A_E is the electrode surface area, ϕ_A is the current efficiency for reactant A, R is the universal gas constant, T is the absolute temperature, n_S is the

number of electrons transferred in the solvent reduction reaction, F is Faraday's constant, and P is the pressure in the gas phase. Pressure was assumed to be close to 101.325 kPa and subject to the ideal gas law. The term $(1 - \phi_A)$ in Eq. 3 was assumed to be approximately one in the case of solvent decomposition, because solvent is present in great excess when compared with other constituents. This assumption allowed Q_g to be calculated without prior knowledge of the current efficiency.

Effect of gas evolution on dispersion

The model may describe the extent of mixing in the FTER cathode compartment by the dispersion coefficient, D. Under gas-evolving conditions, the extent of mixing is bounded by the theoretical limits for plug flow ($D \to 0$) and perfect mixing ($D \to \infty$).[24] No reports of theoretical developments for dispersion in similar physical systems were found in the literature. Therefore, values for D used in the model were measured directly from the tracer experiments performed in this study.

Effect of gas generation on mass transfer

The mass transfer of a reacting species from a bulk fluid to an electrode surface may be impacted by the mechanics of bubble formation, detachment, and ascension. Sedahmed and Shemilt[16] developed an empirical model for the mass transfer coefficient to hydrogen-evolving mesh electrodes in a quiescent electrolyte. That model was modified to describe the mass transfer coefficient for gas generation-induced flow as

$$k_{mt,g} = a(Q_g)^b \tag{4}$$

where $k_{mt,g}$ is the mass transfer coefficient under gas-evolving conditions, and a and b are fitting parameters. The values of a and b used in this study were for a hydrogen gas-evolving planar metal electrode and were independent of electrode plane orientation relative to gas bubble flow.[16] The parameter values account for the specific mechanism of mass-transfer enhancement.

The contributions of convection and gas generation on the mass transfer of a reactant to the electrode surface were treated by vector addition of their associated mass fluxes. The overall mass transfer coefficient can then be calculated as the vectorial sum of the individual mass transfer coefficient from the two contributing processes.[25]

$$k_{mt} = \sqrt{k_{mt,g}^2 + k_{mt,c}^2} \tag{5}$$

where $k_{mt,c}$ is the mass transfer coefficient corresponding to the condition of only convection (no effect of gas generation) around the mesh electrode, which was determined experimentally. The pseudo-volumetric reaction rate constant (k) in Eq. 1 was related to k_{mt} by

$$k = k_{mt}\frac{A_E}{V_R} \tag{6}$$

where V_R is the reactor volume.

Dimensionless governing equation

To examine the broader implications of extending the model to include gas generation, Eq. 1 was nondimensionalized by introducing a dimensionless length ($\bar{x} = x/L$) and concentration ($\bar{c} = C_A/C_{A,0}$) into the steady-state version of Eq. 1, yielding

$$\frac{d^2\bar{c}}{d\bar{x}^2} = Pe_m\frac{d\bar{c}}{d\bar{x}} + Da_m\bar{c} \tag{7}$$

where Da_m ($= kL^2/D$) is a mixing Damköhler number. Since $k\tau = Da_m/Pe_m$, Eq. 2 was recast to calculate χ in terms of Da_m and Pe_m. Because Da_m and Pe_m are a function of Q and Q_g, this provides a basis to analyze system performance in terms of relative fundamental process rates (i.e., mixing, convection, and reaction).

Current efficiency

Current efficiency and conversion are coupled by the relative reaction rates of each species in the system.[26] A priori determination of current efficiency is important to estimate the power cost at various operating conditions. For this system, with only two reactions—electron transfer to a dilute species and solvent decomposition on the electrode leading to gas evolution—current efficiency was defined as

$$\phi_A = \frac{j_A}{j_A + j_S} \tag{8}$$

where j_A is the current density attributable to the reaction of species A and j_S is the current density attributable to solvent decomposition.

Two assumptions were made to cast j_A and j_S in terms of experimentally controlled parameters. First, the rate of solvent decomposition was assumed to be linearly dependent on electrode potential. Given this, j_S may be calculated by the linear approximation of the Tafel equation.

$$j_S = -j_{0,S}\frac{n_S F}{RT}\left(\psi_C - E_S^0\right) \tag{9}$$

where $j_{0,S}$ is the exchange current density of the solvent, ψ_c is the cathode potential relative to the standard hydrogen electrode (SHE), and E_S^0 is the standard reduction potential of the $H_2O/H_2,OH^-$ couple relative to SHE.[27] The second assumption was that the reaction rate of the dilute species was controlled only by mass transport to the electrode surface. This assumption applies to cases in which the standard redox potential of the dilute species is much smaller in magnitude than the solvent decomposition potential. Consequently, when solvent decomposition occurs, the dilute species electron transfer kinetics are rapid enough such that mass transfer controls the overall reaction rate.

When these two assumptions were applied, Eq. 8 was expanded to

$$\phi_A = \frac{n_A F k_{mt} C_A^{bulk}/A_E}{n_A F k_{mt} C_A^{bulk}/A_E + j_{0,S} n_S F\left(E_S^0 - \psi_C\right)/RT} \tag{10}$$

where n_A is the moles of electrons transferred in the reaction of species A and C_A^{bulk} is the concentration of species A in the bulk phase.

Experimental

Materials

Potassium ferricyanide (Fisher, ACS grade), potassium ferrocyanide trihydrate (Acros, ACS grade), anhydrous potassium phosphate dibasic (Fisher, ACS grade), potassium phosphate monobasic (Fisher, enzyme grade), *N*-phenylanthranilic acid (Acros, 98% purity), and cerium(IV) sulfate tetrahydrate (Acros, 99+% purity) were purchased and used without further purification. Concentrated hydrochloric acid (Mallinckrodt) and solid phase sodium hydroxide (Fisher, ACS grade) were used to make diluted acid and base solutions. All experimental and analytical method solutions were created using deionized water.

Equipment description

Experiments conducted to determine system parameters and validate the process model were carried out using a laboratory-scale FTER constructed within a 20 cm long by 5 cm ID Plexiglass column (Figure 1). The electrode assembly was constructed with an expanded titanium mesh coated with mixed metal oxides (Elgard 150 Anode Ribbon Mesh, Corrpro Companies) as the electrodes. The surface area of the electrodes (A_E) was 50 cm^2. Layers of Geonet and Geotextile (Tenax, Baltimore, MD), two inert, nonconductive, high-density polyethylene materials, were used to separate the electrodes, provide open space for gas bubbles to freely ascend, and keep sand from infiltrating the assembly. A Nytex screen (Wildco, Buffalo, NY) was placed between the electrodes to separate the cathode section from the gas evolution effects of the anode section. The assembly volume was approximately 39 cm^3. The remainder of the column was packed with clean quartz-feldspar sand as a representative soil.

Power was applied to the electrodes using a GW Laboratory DC Power Supply (model GPS-3030D) in a constant current mode. Electrode potentials were measured relative to Ag/AgCl reference electrodes (World Precision Instruments, Sarasota, FL) placed about 0.5 cm from the electrode surface. Electrode potentials were recorded at 60 s intervals with LabView 7.0 Express (National Instruments, Austin, TX) using a National Instruments PCI-6024E data acquisition device. Gas was vented through a port at the top of the electrode assembly attached to a Tedlar bag (SKC, Eighty Four, PA) with a Tygon hose. The feedstock and effluent solutions were stored in 1 L Erlenmeyer flasks. The solution was pumped through the column using an Ismatec Reglo analog compact multichannel variable speed pump (Switzerland) and all connections were made with Viton and Teflon tubing (VWR, Vernon Hills, IL).

Transient experiments

The extent of mixing within the electrode assembly as a function of gas evolution rate and liquid flowrate was evaluated using transient tracer tests. Breakthrough curves as a result of a step increase in $Fe(CN)_6^{3-}$ concentration from 0 to 5 mmol/L were measured for three volumetric flowrates (0.1, 0.5, and 1.5 cm^3/min) and four applied currents (0, 0.05, 0.1, and 0.2 A). The supporting electrolyte for all experiments was an aqueous 0.1 mol/L KH_2PO_4/Na_2HPO_4 buffer solution (pH 7). Column effluent samples were acquired at 10–60 min intervals, depending on the flowrate, and stored in 2 cm^3 glass vials at room temperature (22°C) in the dark.

The dispersion coefficient at different gas generation rates was estimated using conservative tracer methods. Starting with Eq. 1 for a conserved species, the response in effluent concentration to a step input of the tracer concentration from zero to $C_{T,0}$, introduced at the reactor inlet,[14] is

$$C_T(L,t) = \frac{C_{T,0}}{2}\operatorname{erfc}\left(\frac{L-ut}{\sqrt{4Dt}}\right) \tag{11}$$

Equation 11 is valid at large Pe_m (>100) for both open and closed boundary conditions.

To reconcile the fact that ferricyanide was converted through the system, it was recognized that the ferrocyanide production rate was equal to the rate of ferricyanide consumption. Consequently, a governing equation for the tracer in terms of the combined ferricyanide and ferrocyanide molar concentration was utilized. The breakthrough curve of $Fe(CN)_6^{3-} + Fe(CN)_6^{4-}$ molar concentration was fit using Eq. 11 to determine D as a function of experimental conditions. Molecular diffusion of each individual compound is treated as independent of other solutes under dilute solution assumptions. However, diffusion is typically only a minor contribution to the overall magnitude of the dispersion coefficient. This assumption was utilized to allow breakthrough curves analysis using the total $Fe(CN)_6^{3-} + Fe(CN)_6^{4-}$ species balance equation. Because liquid void fraction within the system was a function of Q_g (i.e., I), the mean residence time ($C_T/C_{T,0} = 0.5$) changed over the experimental conditions. Therefore, to improve the data regression fit, u was also used as a fitting parameter. Regression was performed in Mathcad 12.0 with the Levenburg-Marquardt nonlinear regression package.

Steady-state experiments

System performance, expressed as ferricyanide conversion (χ) and current efficiency (ϕ), was evaluated in steady-state column experiments. The flow rate and current conditions were the same as those used in the transient experiments. The steady-state conversion and current efficiency for ferricyanide were calculated for each pore volume through the system after effluent concentrations were constant (~2 to 3 pore volumes). The reported conversion and current efficiency were averages of the three to four calculations at steady-state.

Additional steady-state experiments were performed in the absence of gas generation to estimate the convective mass transfer coefficient ($k_{mt,c}$) as a function of flow rate. The cathode potential was set from −0.4 to −0.5 V vs. SHE, approximately one volt more negative than the $Fe(CN)_6^{3-}/Fe(CN)_6^{4-}$ standard reduction potential, but not sufficiently negative to produce H_2 gas. Because no gas was generated, $k_{mt} = k_{mt,c}$. The convective mass transfer coefficient was

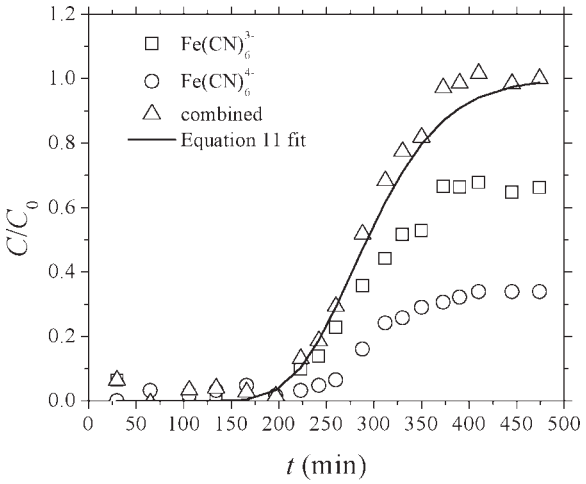

Figure 2. Multicomponenent breakthough curve at Q = 0.5 cm^3/min and I = 0.1 A.

Solid line is the regression fit of Eq. 4 to the total molar concentration data.

determined using the steady-state conversion with Eqs. 2 and 6. The value for D was taken from the no-current control transient experiments (0.005 cm^2/min).

Analytical methods

Ferricyanide concentrations were determined by visible light absorbance at 470 nm using a Perkin-Elmer model 124 double-beam spectrophotometer. Concentrations were calculated by comparing the absorbance to standard solutions (0–7.5 mmol/L) of $Fe(CN)_6^{3-}$ in 100 mmol/L pH 7 phosphate buffer solution. The ferricyanide detection limit of the spectrophotometric method was 0.05 mmol/L. Ferrocyanide concentrations were determined by redox titration with cerium(IV) sulfate to an E_h of 0.905 V vs. SHE using *N*-phenylanthranilic acid as an end-point indicator. The ferrocyanide detection limit using the redox titration was 0.1 mmol/L. The lack of ferrocyanide absorbance interference and ferricyanide titration interference was verified before conducting tracer experiments.

Results and Discussion

Impact of operating conditions on dispersion

Breakthrough tests were initially performed to determine D in the absence of current to verify that there were no preferential flow paths through the column. The calculated D from the $Fe(CN)_6^{3-}$ breakthrough curve was 0.005 cm^2/min. The breakthrough curve was absent of peaks or a long tail, indicating that the column was well packed.

The response to the step increase in $Fe(CN)_6^{3-}$ influent concentration was adequately described using Eq. 11 for the entire range of conditions analyzed in the transient, gas-evolving tracer experiments (Figure 2). In some cases, the value of Pe_m through the entire column was smaller than 100, beyond the generally accepted limit of applicability for Eq. 11.[24] An alternative method, in which the derivative of the step response curve was analyzed as an impulse-type tracer experiment, was also used to calculate D. This second approach resulted in values within one standard deviation of those from the original calculations, and therefore, the values from the original method were used in the subsequent analyses.

Mixing within the reactor was a function of both current (which affection the gas evolution rate) and the nominal volumetric flow rate through the system (Table 1). The mean residence times ($t_{0.5}$) decreased, as expected, with increasing flowrates, but were variable with respect to changes in I (Table 1). This variability may have been due to the random nature of the bubble-induced mixing or changes in pump tubing elasticity over time. At the highest Q_g, ~0.03 cm^3/(cm^2 min), the values of D began to converge. Similar results were reported by Wu et al.[23] This suggested that gas evolution controlled the hydrodynamics when Q_g was 0.03 cm^3/(cm^2 min). Conversely, at lower Q_g values, convective flow through the system controlled the hydrodynamics within the electrode assembly. This was indicated by the larger range of D values at the lower Q_g over the range of nominal flowrates evaluated.

Impact of operating conditions on mass transfer

Ferricyanide reduction under mass transfer-controlled conditions in the absence of gas evolution was evaluated to determine $k_{mt,c}$ as a function of the nominal flowrate. The convective mass transfer coefficient increased, from 3.5×10^{-5} to 1.26×10^{-4} cm/s, with increasing nominal flowrate (0.1–1.5 cm^3/min) following a power law model ($k_{mt,c} \propto Q^{0.3}$). It is notable that the exponent 0.3 is close to the theoretical value of 0.33 in Sherwood number correlations with respect to Reynolds number for a submerged object in the creeping flow regime.[28]

Surface area-normalized gas evolution rates as a function of I were calculated using Eq. 3 (Table 1). The normalized rates were used to calculate $k_{mt,g}$ using Eq. 4 ($a = 3.25 \times 10^{-4}$ cm/s, $b = 0.19$), and are presented in Figure 3a as a function of I. The overall mass transfer coefficient, k_{mt}, was calculated by Eq. 5 for each experimental condition

Table 1. Mean Residence Time and Dispersion Coefficient as a Function of Flowrate and Applied Current or Gas Evolution Rate

	I = 0.05 A		I = 0.1 A		I = 0.2 A	
	Q_g = 0.007 cm^3/(cm^2 min)		Q_g = 0.015 cm^3/(cm^2 min)		Q_g = 0.030 cm^3/(cm^2 min)	
Q (cm^3/min)	$t_{0.5}$ (min)	D (cm^2/min)	$t_{0.5}$ (min)	D (cm^2/min)	$t_{0.5}$ (min)	D (cm^2/min)
0.1	1286	0.021 ± 0.005	1638	0.0061 ± 0.0009	1425	0.014 ± 0.002
0.5	293	0.032 ± 0.003	330	0.049 ± 0.008	376	0.101 ± 0.014
1.5	110	0.231 ± 0.041	103	0.256 ± 0.058	88	0.164 ± 0.059

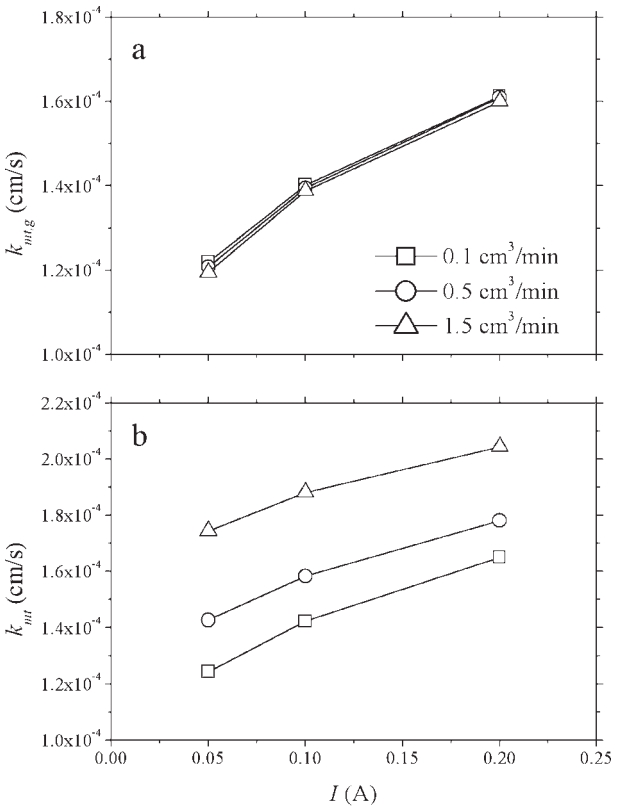

Figure 3. Mass-transfer coefficient due to (a) pure gas evolution, and (b) mass-transfer coefficient with convection and gas evolution contribution.

evaluated (Figure 3b). Values of k_{mt} begin to plateau and slightly converge as Q_g (or I) was increased. This further suggests that as Q_g increases, it becomes the dominant mass transport process (relative to Q).

Comparison of experimental and predicted conversion

Ferricyanide conversion was calculated from the steady-state experimental results and compared with predictions using Eq. 2. Two sets of calculations were performed. The first set of calculations incorporated contributions from gas generation into D and k (extended model). Dispersion coefficients determined from the reactive tracer experiments were divided by 2, to account for the tracer passing through two gas-generating electrode chambers, and substituted into Eq. 2. Assuming that each section behaved independently of the other, the dispersion coefficients are additive.[24] Equal dispersion between sections was a conservative estimate of the distribution based on the equal section residence times. The second set of calculations (basic model) disregarded the impact of gas evolution on D and k (i.e., $D = 0.005$ cm^2/min, $k_{mt,g} = 0$). These were performed to assess the contribution of gas evolution on system performance.

The extended model predictions generally matched experimental results when the effects of gas generation were incorporated into the model (Figure 4). Calculations using the basic model assumptions underestimated experimental conversion (Figure 4). It was expected that the best agreement between the experiment and extended model calculations would occur at the largest gas evolution rate ($I = 0.2$ A), when gas generation exhibited the greatest influence on D and k_{mt}. The close agreement was not observed at 0.2 A, and experimental results were consistently lower than the expected conversion, although experimental variability was highest at this condition.

One cause for the lower than expected reactant conversion at high I was the formation of a secondary reaction product, most likely the mixed-valent compound Prussian blue.[29] Blue deposits were observed on the electrode surface after experiments were performed at 0.2 A. A combination of cycling the electrode polarities and flushing the electrode assembly through the column ports nearest the assembly appeared to remove the majority of deposits.

At the lowest liquid flow rate, where D was relatively small and system performance was expected to be analogous to a PFR, the extended model predictions at low Q_g ($I = 0.05$ A) compared well with the experimental results relative

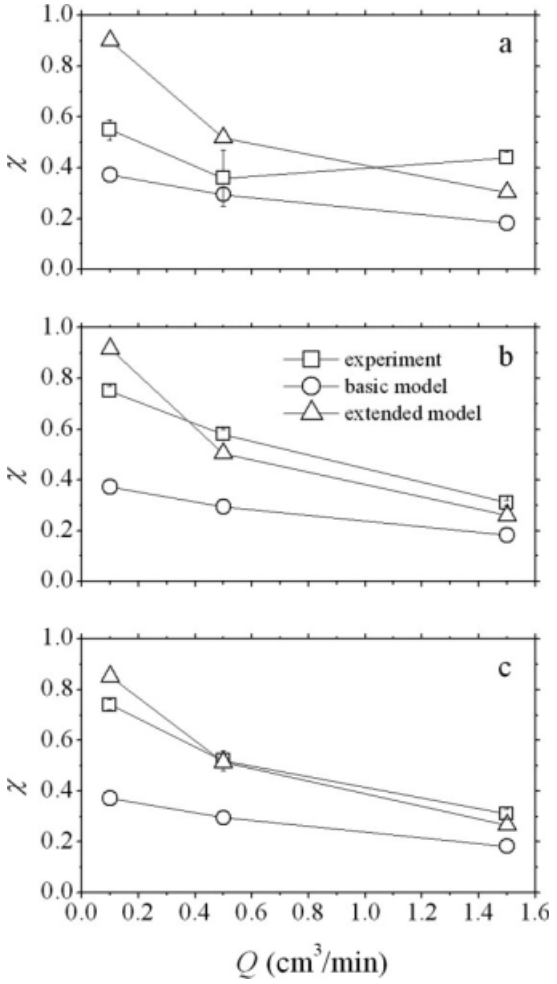

Figure 4. Conversion as a function of liquid flowrate (*Q*) at (a) *I* = 0.2 A, (b) *I* = 0.1 A, and (c) *I* = 0.05 A.

Experimental data error bars represent one standard deviation of the average conversion.

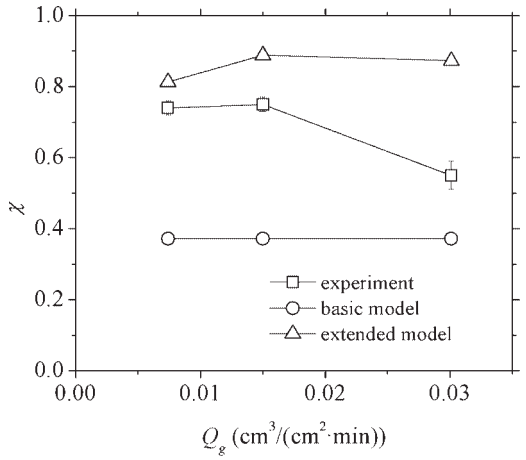

Figure 5. Predicted and measured conversion at three surface area normalized gas generation rates for Q = 0.1 cm³/min.

Experimental data error bars represent one standard deviation of the average conversion.

to the basic model (Figure 5). The experimental conversion exhibited a local maximum over the current range evaluated. This local maximum may be due to the relative contribution of gas generation toward mixing and mass transfer. Moderate gas generation rates may strike a balance between these two mechanisms that affect conversion oppositely (i.e., increased mixing decreases conversion and increased mass transfer increases conversion). This concept is explored in the following section.

Although the agreement was poor between the experiment and extended model at $Q_g = 0.03$ cm³/(cm² min), the overall results illustrate the necessity to incorporate gas generation into the process model formulation. Integrating gas generation imparts flexibility into the model that allows the variable mixing and mass transfer effects to be captured.

Experimental and predicted current efficiency

Values of the current efficiency for $Fe(CN)_6^{3-}$ reduction calculated from Eq. 10 and those determined experimentally determined decreased with decreasing electrode potentials (Figure 6). Equation 10 overestimated ϕ by 0.15–0.25 at cathode potentials near E_s^0. Competing reactants such as dissolved O_2 and alterative reactions may have contributed to the overall current at more positive potentials, decreasing $Fe(CN)_6^{3-}$ reduction efficiency. At more negative potentials, the rate of alternative water reduction pathways would be suppressed by the larger driving force of H_2O reduction directed toward H_2 evolution.

The form of Eq. 10 dictates that ϕ for a mass-transfer controlled reaction will decay as $|\psi_c|$ increases by $(1 + |\psi_c|)^{-1}$. Therefore, ϕ will generally decrease when efforts are made to increase the rate of reduction by lowering ψ_c. This trend impacts the economic sustainability of an FTER implementation because low efficiency processes would consume more power to treat the same contaminant flux as those of higher efficiency systems. Because of the small aqueous solubility of most organic groundwater contaminants, dissolved concentrations are often low (< 1 mmol/L). Therefore, the electron cost for 100% conversion is small under most circumstances. Consequently, the energy input cost as ϕ approaches zero may still be competitive with other PRB technologies.[30]

Dimensional analysis

The dimensionless numbers Pe_m and Da_m are both functions of u and Q_g (via k and D). Therefore, all of the processes characterized by Pe_m and Da_m are coupled, constricting the range of possible system operating conditions.

A localized weighted polynomial regression (loess localized regression function in Mathcad 12.0) was used to calculate D over the experimental parameter range (u and Q_g). The empirical model was utilized with a given range of Da_m values centered on 1 to calculate corresponding values of Pe_m for specific Q and Q_g (Figure 7). As Q decreased, lines of constant Q_g separated and decreased for the same Q_g, indicating an increased impact of gas evolution on transport processes. This suggests that a larger degree of mixing dictates the operating conditions, possibly limiting χ. Conversion under this framework was evaluated to investigate the competing effects of gas evolution influenced mixing and mass transfer.

Values of χ were calculated for the sets of (Da_m, Pe_m) pairs at constant Q and Q_g using Eq. 2 (Table 2). The spread between lines of constant Q_g in Figure 7 were reproduced in the χ calculations. Conversion was maximized at the smallest Q and largest Q_g. These conditions correspond to (Da_m, Pe_m) pairs in the upper right quadrants of Figure 7a through 7c. In this region of the operating domain, the dominant mechanisms are the mass-transfer controlled reaction rate and convective transport through the assembly. Therefore, the relative impact of gas generation is greater toward enhancing mass transfer to the electrode surface than inducing mixing within the assembly.

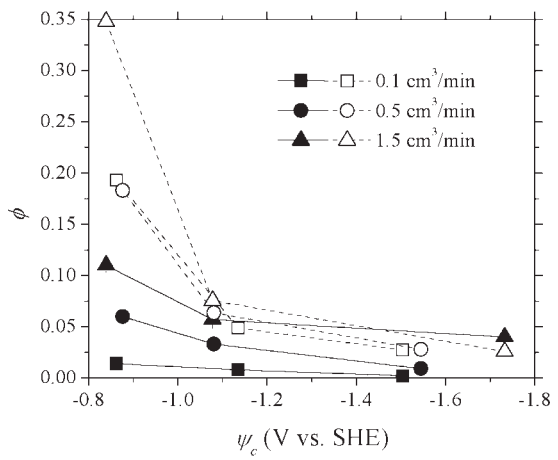

Figure 6. Measured (closed symbols—solid line) and predicted (open symbols—dashed line) current efficiency as a function of flowrate and cathode potential.

Experimental data error bars represent one standard deviation of the average conversion.

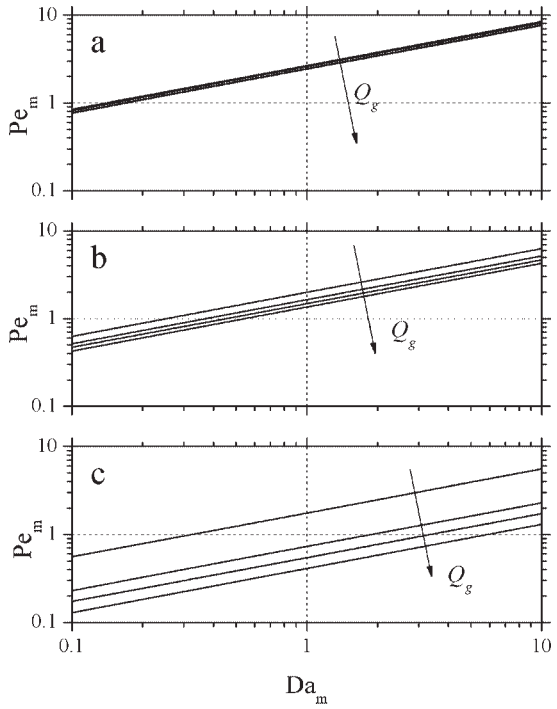

Figure 7. Lines of constant Q_g from decreasing to increasing rates in the direction of the arrow; Da_m and corresponding Pe_m numbers were calculated for Q_g = 0.007, 0.016, 0.022, and 0.03 cm^3/(cm^2 min).

Dimensionless numbers were calculated at three volumetric flowrates (a) 1.5 cm^3/min, (b) 0.5 cm^3/min, and (c) 0.1 cm^3/min.

The continuum assumption within the electrode assembly was reconsidered in an effort to improve model accuracy. Under this assumption, reactions are considered to proceed uniformly within the reactor volume. The discrepancy between the assumed system and actual spatially nonuniform conditions in heterogeneous reactors has been treated by others using a catalyst-phase contact time distribution.[31,32] This has been used to explain χ overestimation in heterogeneous reactors when a classical residence time distribution (RTD) was first applied. The present system differs from those considered in Tayakout-Fayolle et al.[32] because reactions proceeded only on the electrode surface, and not in a separate catalyst phase (e.g., porous catalyst pellet). The probability of reactant contact with the electrode depends on the overall RTD. Although deconvoluting this relationship through experimental methods is a challenge, this concept was utilized to qualitatively evaluate the model prediction accuracy.

The largest extended model-experimental discrepancies (average difference = 0.19) were at Q = 0.1 cm^3/min (Figure 4). At this flow rate, mixing tended to be the dominate transport mechanism. Consequently, the continuum assumption in the well-mixed system would break down because reactants are less available for diffusion to the electrode when concentrations are more evenly distributed. As plug-flow characteristics become prevalent, the continuum assumption appears to remain valid. This was confirmed by the good agreement between model and experiment at the higher flow rate (average difference = 0.07; two conditions were statistically identical at the 95% confidence level).

Conclusions

Performance of a novel electrolytic PRB system was analyzed using a reactor model extended to incorporate the effect of gas generation on multiple transport mechanisms. Mixing within the electrode assembly was experimentally determined at different flow rates through the system and electrolytic gas generation rates. Although discrepancies existed between experimental and predicted conversions, operating condition trends were suitably predicted with the model. The approach to scale-up this system for field deployment is to increase the vertical height of the electrode assembly, which is parallel to flow through the assembly. A consequence of this approach is that the dominant

Table 2. Predicted Conversion as a Function of Da_m and Pe_m Pairs at Constant Liquid Flowrate and Gas Generation Rate

		At Q_g = 0.07 cm^3/(cm^2 min)		At Q_g = 0.016 cm^3/(cm^2 min)		At Q_g = 0.022 cm^3/(cm^2 min)		At Q_g = 0.03 cm^3/(cm^2 min)	
Q (cm^3/min)	Da_m	Pe_m	χ_A	Pe_m	χ_A	Pe_m	χ_A	Pe_m	χ_A
0.1	0.1	0.56	0.15	0.23	0.31	0.17	0.37	0.13	0.44
	0.5	1.25	0.30	0.52	0.51	0.39	0.58	0.29	0.65
	1	1.76	0.39	0.73	0.61	0.55	0.68	0.41	0.74
	5	3.94	0.65	1.63	0.84	1.22	0.88	0.92	0.91
	10	5.57	0.77	2.31	0.92	1.73	0.94	1.30	0.96
0.5	0.1	0.63	0.14	0.52	0.16	0.47	0.18	0.43	0.19
	0.5	1.41	0.27	1.16	0.31	1.05	0.34	0.96	0.36
	1	1.99	0.36	1.64	0.41	1.48	0.43	1.35	0.45
	5	4.45	0.62	3.66	0.67	3.31	0.70	3.02	0.72
	10	6.30	0.74	5.18	0.79	4.69	0.81	4.27	0.83
1.5	0.1	0.82	0.11	0.77	0.12	0.78	0.12	0.84	0.11
	0.5	1.83	0.22	1.71	0.24	1.74	0.23	1.89	0.22
	1	2.58	0.30	2.42	0.31	2.45	0.31	2.67	0.29
	5	5.78	0.54	5.42	0.56	5.49	0.56	5.97	0.53
	10	8.17	0.67	7.66	0.68	7.76	0.68	8.44	0.66

component of convective flow will be parallel to the planar mesh over a larger portion of the electrodes when compared with the experimental system. This is expected to specifically impact the extended model by affecting the mass-transport coefficient because the expression utilized in this work was developed under quiescent mixing conditions. Other challenges of applying the extended model to large-scale systems include accounting for nonuniformities in convective flow imposed by aquifer heterogeneities and the impact of more complex chemical systems that may not be mass transfer rate limited. Although these challenges are recognized, the processes identified in this work are expected to remain critical to elucidating system performance at the larger scale.

Acknowledgements

The authors gratefully acknowledge the contribution of Dr. Tom Sale for his contribution to the manuscript. This research was partially funded through the University Consortium for Field Focused Groundwater Contamination Research.

Literature Cited

1. Gillham RW, O'Hannesin S. Enhanced degradation of halogenated aliphatics by zero-valent iron. *Ground Water*. 1994;32:958–967.
2. Matheson LJ, Tratnyek PG. Reductive dehalogenation of chlorinated methanes by iron metal. *Environ Sci Technol*. 1994;28:2045–2053.
3. Gilbert DM, Sale TC. Sequential electrolytic oxidation and reduction of aqueous phase energetic compounds. *Environ Sci Technol*. 2005;39:9270–9277.
4. Wani AH, O'Neal BR, Gilbert DM, Gent DB, Davis JL. Electrolytic transformation of ordinance related compounds (ORCs) in groundwater: laboratory mass nalance studies. *Chemosphere*. 2006;62:689–698.
5. Petersen MA, Sale TC, Reardon KF. Electrolytic trichloroethene degradation using mixed metal oxide coated titanium mesh electrodes. *Chemosphere*. 2007;67:1573–1581.
6. Starr RC, Cherry JA. In situ remediation of contaminated ground water: the funnel-and-gate system. *Ground Water*. 1994;32:465–476.
7. Yabusaki S, Cantrell K, Sass B, Steefel C. Multicomponent reactive transport in an in situ zero-valent iron cell. *Environ Sci Technol*. 2001;35:1493–1503.
8. Hatfield K, Burris DR, Wolfe NL. Analytical model for heterogeneous reactions in mixed porous media. *J Environ Eng*. 1996;122:676–684.
9. Rabideau AJ, Suribhatla R, Craig JR. Analytical models for the design of iron-based permeable reactive barriers. *J Environ Eng*. 2005;131:1589–1597.
10. Fryar AE, Schwartz FW. Hydraulic-conductivity reduction, reaction-front propagation, and preferential flow within a model reactive barrier. *J Contam Hydrol*. 1998;32:333–351.
11. Kamolpornwijit W, Liang L, West OR, Moline GR, Sullivan AB. Preferential flow path development and its influence on long-term PRB performance: column study. *J Contam Hydrol*. 2003;66:161–178.
12. Liang L, Moline GR, Kamolpornwijit W, West OR. Influence of hydrogeochemical processes on zero-valent iron reactive barrier performance: a field investigation. *J Contam Hydrol*. 2005;78:291–312.
13. Painter BDM. Reactive barriers: hydraulic performance and design enhancements. *Ground Water*. 2004;42:609–617.
14. Danckwerts PV. Continuous flow systems. *Chem Eng Sci*. 1953;2:1–18.
15. Sedahmed GH. Mass transfer at packed-bed, gas-evolving electrodes. *J Appl Electrochem*. 1987;17:746–752.
16. Sedahmed GH, Shemilt LW. Mass transfer characteristics of electrochemical reactors employing gas evolving mesh electrodes. *J Appl Electrochem*. 1984;14:123–130.
17. Shah A, Jorne J. Mass transfer under bubble-induced convection in a vertical electrochemical cell. *J Electrochem Soc*. 1989;136:144–153.
18. Vogt H. Mechanisms of mass transfer of dissolved gas from a gas-evolving electrode and their effect on mass transfer coefficient and concentration overpotential. *J Appl Electrochem*. 1989;19:713–719.
19. Bisang JM. Effect of mass transfer on the current distribution in monopolar and bipolar electrochemical reactors with a gas-evolving electrode. *J Appl Electrochem*. 1993;23:966–974.
20. Janssen LJJ. Mass transfer at gas-evolving vertical electrodes. *J Appl Electrochem*. 1987;17:1177–1189.
21. Shah A, Jorne J. Mass transfer under combined gas evolution and forced convection. *J Electrochem Soc*. 1989;136:153–158.
22. Wu WS, Rangaiah GP. Effect of gas evolution on mass transfer in an electrochemical reactor. *J Appl Electrochem*. 1993;23:1139–1146.
23. Wu WS, Rangaiah GP, Fleischmann M. Effect of gas evolution on dispersion in an electrochemical reactor. *J Appl Electrochem*. 1993;23:113–119.
24. Levenspiel O. *Chemical Reaction Engineering*, 3rd ed. New York: Wiley, 1999.
25. Wendt H, Kreysa G. *Electrochemical Engineering: Science and Technology in Chemical and Other Industries*. Berlin: Springer, 1999.
26. Sterten Å, Solli PA. An electrochemical current efficiency model for aluminium electrolysis cells. *J Appl Electrochem*. 1996;26:187–193.
27. Bard AJ, Faulkner LR. *Electrochemical Methods: Fundamentals and Applications*, 2nd ed. New York: Wiley, 2001.
28. Bird RB, Stewart WE, Lightfoot EN. *Transport Phenomena*, 2nd ed. New York: Wiley, 2002.
29. Ogura K, Nakayama M, Nakaoka K. Electrochemical quartz crystal microbalance and in situ infrared spectroscopic studies on the redox reaction of prussian blue. *J Electroanal Chem*. 1999;474:101–106.
30. Sale T, Petersen M, Gilbert D. Final Report: Electrically Induced Redox Barriers for Treatment of Groundwater (CU-0112). ESTCP Project Number CU-0112. 2005.
31. Shinnar R, Naor P, Katz S. Interpretation and evaluation of multiple tracer experiments. *Chem Eng Sci*. 1972;27:1627–1642.
32. Tayakout-Fayolle M, Othman S, Jallut C. A new technique for the determination of contact time distribution (CTD) from tracer experiments in heterogeneous systems. *Chem Eng Sci*. 2005;60:4623–4633.

Manuscript received Mar. 15, 2008, and revision received Jan. 7, 2009.